AIAA 2002-2194
2-D Magnetohydrodynamic Modeling of a Pulsed Plasma Thruster

Y. C. F. Thio
NASA Marshall Space Flight Center
Huntsville, Alabama

J. T. Cassibry, S. T. Wu
University of Alabama in Huntsville
Alabama

33rd AIAA Plasmadynamics and Lasers Conference
20-23 May 2002 / Maui, Hawaii

AIAA-2002-2194

2-D Magnetohydrodynamic Modeling of a Pulsed Plasma Thruster

Y. C. Francis Thio, Jason T. Cassibry[1], S. T. Wu*
NASA Marshall Space Flight Center

Abstract

Experiments are being performed on the NASA Marshall Space Flight Center (MSFC) MK-1 pulsed plasma thruster [1]. Data produced from the experiments provide an opportunity to further understand the plasma dynamics in these thrusters via detailed computational modeling. The detailed and accurate understanding of the plasma dynamics in these devices holds the key towards extending their capabilities in a number of applications, including their applications as high power (> 1 MW) thrusters, and their use for producing high-velocity, uniform plasma jets for experimental purposes. For this study, the 2-D MHD modeling code, MACH2, is used to provide detailed interpretation of the experimental data. At the same time, a 0-D physics model of the plasma initial phase is developed to guide our 2-D modeling studies.

Introduction

A coaxial pulsed plasma thruster (PPT) is a plasma accelerator consisting of a pair of coaxial cylindrical electrodes. Current from a capacitor bank enters at one of the electrodes, crossing the gap between the electrodes through a plasma, and returns to the capacitor bank via the other electrode. The current following in the electrodes generates an azimuthal magnetic field in the region between the electrodes. This magnetic field acts on the plasma current to produce the electromagnetic $\mathbf{j} \times \mathbf{B}$ (Lorentz) force on the plasma, accelerating the plasma down the tube. At least that is the original concept. In a real device, the PPT displays a wide range of complexity in the plasma behavior. Detailed magneto-plasma dynamic modeling provides the means to understand this complexity, and hence to improve its performance.

Despite the fact that research and development of pulsed plasma thrusters has been conducted for more than 40 years[1-3], magnetohydrodynamic (MHD) modeling using two or more spatial dimensions to analyze the detailed plasmadynamic behavior of pulsed plasma thrusters and comparing the modeling results with experiments has been few and far between. The work of Keefer[4] involving the use of a sophisticated MHD code such as MACH2[5] to the modeling of plasma thrusters is a relatively recent event. Mikellides has applied the code to model related but very different devices, the MPD thrusters[6-10]. A recent study was made by Shen and co-workers[11]. Sankaran is developing a new 2-D MHD code for modeling MHD flows in similar thrusters[12]. Earlier work includes those of Andrenucci[13] and Ao [14].

At the NASA Marshall Space Flight Center, a new pulsed power laboratory (Figure 1) has been developed to undertake research of transient processes occurring in high energy density plasmas. Developing the experimental infrastructure of the laboratory involves the development and testing of the pulsed power supply (a capacitor bank) and its transmission manifold, the high-voltage charging power supply, the control and firing subsystem, a fast and low-jitter trigger generator, the multi-channel data acquisition system and the plasma diagnostics. A pulsed plasma device serving as an electrical load as well as a switch for the testing and commissioning of the pulsed power experimental system is required. Since the immediate application of the pulsed power laboratory is to conduct research in support of magnetized target fusion propulsion driven by high-velocity plasma guns[15], a device involving plasma acceleration of some kind would be useful as an electrical load for the test. The result was a coaxial plasma acceleration device that was given the name the Mark-1 plasma gun.

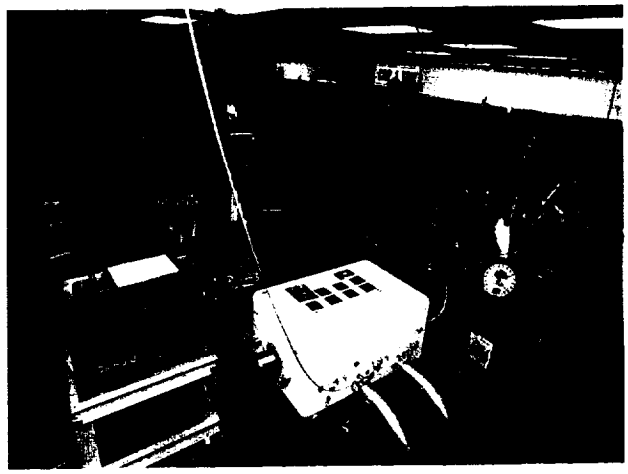

Figure 1. The new pulsed power laboratory at NASA Marshall Space Flight Center.

Nevertheless, the working of the plasma gun is similar to a pulsed plasma thruster, and thus provided an

[1] University of Alabama, Huntsville, USA.

opportunity for studying the plasma dynamics in a coaxial pulsed plasma thruster. In particular, it provides the opportunity of benchmarking our computer models against experimental data. It has become a rather useful device that aids in the design of our principal research accelerator (now called the Mark-2 plasma gun), besides serving an electrical load for the development of the experimental infrastructure. As a design tool for the Mark-2 gun, we are in the process of adding and testing other features on this gun that we plan to incorporate in the Mark-2 gun. The performance and the modeling of these new features will be reported at a later time. This paper serves as an interim progress report in that respect.

The Experimental System

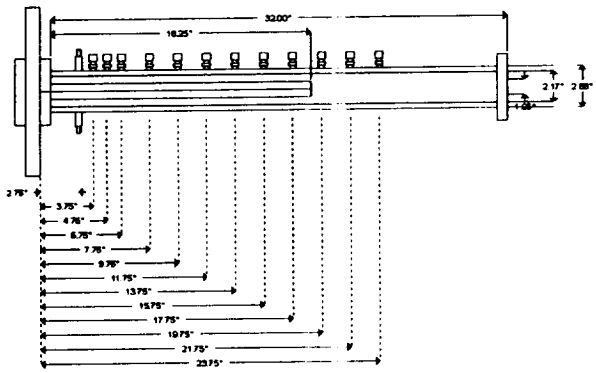

Figure 2. The experimental device (the Mark-1 Gun), consisting of a pair of coaxial cylindrical electrodes.

The Mark-1 plasma gun consists of a pair of coaxial cylindrical electrodes. The inner electrode has a diameter of 2.667 cm (1.05 in.) and is 0.4635 m (18.25 in.) long measured from the breech plug. The outer electrode has a diameter of 5.398 cm (2.125 in.) and is 0.8128 m long measured from the same breech plug. The plasma gun is connected directly to a pair of capacitors of 330 μF each, via a pair of transmission plates with a total inductance estimated at 230 nH without the use of any external switches. The capacitors are rated for 10 kV maximum voltage, though experiments to-date have been conducted with voltage below 6 kV.

At 6.985 cm (2.75 in.) from the breech plug is a set of six ordinary automobile spark plugs. The bent tip of the outer spark terminal is clipped flushed with the outer casing, so that the spark plug has the geometry of a miniature coaxial plasma gun. The spark plugs are inserted into the outer electrode of the main accelerator through Swedgelok fasteners. These spark plugs are used for initiating the capacitive discharge.

The gun is equipped with a number of diagnostic ports (holes) along its length. They have been used for holding light pipes and magnetic (b-dot) probes. One set of ports are used for laser interferometry for electron density measurements. A set of six light pipes for in-bore optical emission monitoring and five magnetic probes were used in the series of tests just completed.

The plasma gun is physically connected and sealed to a hemispherical vacuum chamber (Figure 3). The vacuum chamber is equipped with a number of diagnostic ports. One port is used for taking high-speed photograph of the plasma jet launched from the thruster. One port is used for making optical emission spectroscopy. One port is used for a set of five light pipes focused at points in the chamber along the axis of the plasma thruster. These light pipes are used to measure the velocity of the plasma jet as it travels through the central portion of the chamber. The interferometric, spectroscopic and photographic measurements will be reported elsewhere. In this paper we shall report and analyse the mainly the in-bore magnetic probes measurement.

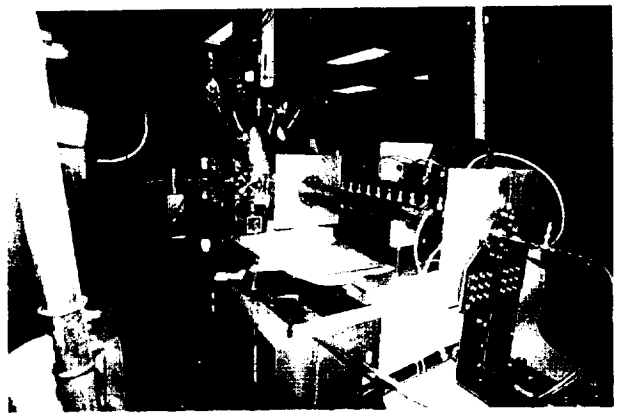

Figure 3. The experimental system showing the pulsed plasma thruster connected to a hemispherical vacuum chamber. The vacuum chamber and the length of the plasma thruster is equipped with a number of diagnostics ports.

The Plasma Initiation Phase

More than a hundred shots have been taken with the Mark-1 gun. One characteristic of the experimental system is that it has been very reliable and its performance is very reproducible. Essentially identical experimental results are obtained with identical charging voltages on the capacitors.

We will select one of the more recent test shots for a detailed discussion. This shot was labeled Shot 2002-03-

0.46% Ar. The part of the breech between the outer and inner electrode exposed to the plasma is a Teflon insulator for this shot. The capacitor is charged to a voltage of 5.36 ± 0.2 kV. The capacitive discharge was initiated by a sharp pulse (~ 5 ns) of current (~ 300 A) and voltage (~ 30 kV) to each of the six modified spark plugs (Figure 4). The modified spark plugs function as miniature coaxial plasma guns ejecting a high-velocity stream of charged particles. The energetic electrons and the associated UV radiation further ionize the He gas in the gun bore. As the electrodes are subjected to the high charging voltage, a Townsend avalanche occurs and turns on the main current pulse. In this shot the current reaches a peak of 155 kA at a time of 18 μs, as measured by the first b-dot probe placed near the breech (Figure 7).

Assume an initial temperature of 25 ^{o}C for the pre-filled helium gas, its particle density is estimated as 2.8×10^{20} m^{-3}. According to Kaye and Laby[16], the effective molecular radius of helium for a classical estimate of the molecular mean free path is 2.18×10^{-10} m. According to Chapman and Cowling, a classical estimate of the molecular mean free path is,

$$\lambda = \frac{1}{\sqrt{2}} \frac{1}{n\pi r_m^2},$$

where r_m is the classical molecular radius and n is the particle number density. For above set of parameters, the molecular mean free path in the pre-filled helium gas is estimated to be 1.7 cm, relatively large in terms of the dimension of our plasma thruster.

In 50 ns, the current rises rapidly to about 0.7 kA, producing a magnetic pressure of 40 Pa at the mid point between the electrodes. This pressure is about 40 times greater than the in-bore gas pressure, sufficient to produce a shock wave through the pre-filled gas.

We argue that this shock cannot be collisional in nature, that is it cannot be a hydrodynamic or a collisional hydromagnetic shock wave. For these collisional shock waves, the density of the gas can at most increases by a factor of $(\gamma + 1)/(\gamma - 1)$ or 4 for $\gamma = 5/3$. The magnetic pressure can be balanced by this gas density if the temperature of the gas goes to approximately 0.3 eV. The temperature is not sufficient to produce any significant ionization. Thus for a collisional shock, the pertinent mean free path in determining the thickness and structure of the shock front is that of the neutral particles. As we have seen above, the neutral mean free path is about 1.7 cm and a typical hydrodynamic shock front has a thickness of several (~ 10 times) the mean free path, making the shock front rather broad, about 17 cm.

We conclude that, up to about 50 ns, the shock produced must be of a collisionless magnetic kind. In the case of a collisionless shock, steep gradients of the magnetic field occurs over distances much shorter than the particles mean free path, where large electrical current flows producing the shock. The collisionless shock front is the region through which the initial current flows. In this collisionless shock the density remains more or less constant at the value of the background gas. The shock travels at about 40 km/s. In 50 ns, the front spread to about 2 mm (<< 1.7 cm). The current density is of the order of 1 MA/m^2 and, to balance the magnetic pressure, the corresponding gas temperature needs to be about 10 eV, sufficiently high to produce ionization. Strictly, the concept of temperature is not appropriate here as the plasma is highly non-equilibrium and non-Maxwellian up to this point. We borrow the concept of temperature loosely to indicate the trend of the discussion. The speed at which the Hall current propagates is of the same order as the collisionless shock, about 40 km/s. The plasma dynamic during this phase is highly dominated by particle kinetics. MHD models would not be appropriate during this regime.

The scenario changes rapidly in the next 50 ns. At 100 ns, the current reaches a value of 1.4 kA, the magnetic pressure at the mid-point between the electrodes is now 160 Pa. This pressure is 160 times is large enough to sustain a collisional hydrodynamic shock temperature of more than 1 eV, even if the density increases by a factor 4 over the background gas. At this temperature, sufficient degree of ionization can be sustained, whereby the ion-ion collisions and their mean free paths come into play. At this density and temperature, the ion-ion mean free path is of the order of 1 mm, sufficiently smaller than the thickness of a collisionless shock. The thickness of a collisional shock here (an MHD shock in this case as the shock is dominated by the magnetic pressure and the ion-ion collisions) is about 10 mm (being ~ 10 times the ion-ion mean free path). The collisionless shock front has also spread to about the same extent of ~ 10 mm. Therefore the shock makes a transition from being collisionless to a collisional one.

The corresponding current density is 9×10^5 A/m^2. At this point, a collisional plasma is more or less established. It is then appropriate to proceed with a MHD model for the plasma dynamics. We thus use the conditions deduced from the above 0-D physics reasoning as the initial conditions to start our MACH2 runs to model the experimental results. Specifically, we start the MACH2 run at t = 100 ns, with an initial plasma with the following parameters: The plasma has a

plasma with the following parameters: The plasma has a thickness of 1.26 cm, a temperature of 3.665 eV, and a particle density of 2.78×10^{20} m^{-3}.

We note that with time, the current is not limited to the width of the MHD shock front. Rather it will spread subjected to the diffusion of the magnetic field, the diffusivity of which is governed by the plasma resistivity. Using Braginskii's coefficients, the plasma resistivity may be estimated to be ~ 10^{-4} ohm-m. At a time of 500 ns for example, the skin depth for the magnetic field is about 10 mm, whereas the shock front has diminished to less than 1 mm thick.

The Main Acceleration Phase

Two-Dimensional MHD Simulations using Mach2

Mach2 Physics Description

Mach2 is a 2 ½D multiblock, Arbitrary Lagrangian Eulerian (ALE), resistive magnetohydrodynamic (MHD) code that carries all three spatial components of vectors, but allows no quantity to depend on the coordinate that is normal to the computational plane. Mach2 solves the following dynamical equations in a fractional time-split manner:

Mass Continuity

$$\frac{\partial \rho}{\partial t} = -\nabla \cdot (\rho \vec{v})$$

Fluid Momentum

$$\rho \frac{\partial v^i}{\partial t} = -\rho v^j \nabla_j v^i + \nabla_j \begin{bmatrix} -\left(P + Q + \frac{1}{3} u_R\right)\delta^{ji} \\ +\frac{1}{\mu_0}\left(B^j B^i - \frac{1}{2} B^2 \delta^{ji}\right) \end{bmatrix} + \nabla_j \sigma^{dji}$$

Electron Specific Internal Energy

$$\rho \frac{\partial \epsilon_e}{\partial t} = -\rho \vec{v} \cdot \nabla \epsilon_e - P_e \delta^{ji} \nabla_i v_j + \eta J^2 - \vec{J} \cdot \left(\frac{\nabla P_e}{e n_e}\right) + \nabla \cdot (\kappa_e \nabla T_e) - \Phi_{eR} - \rho \kappa_{ei} \frac{(T_e - T_i)}{\tau_{ei}}$$

Ion Specific Internal Energy

$$\rho \frac{\partial \epsilon_i}{\partial t} = -\rho \vec{v} \cdot \nabla \epsilon_i + \left[-(P_i + Q)\delta^{ji} + \sigma^{dji}\right] \nabla_i v_j + \nabla \cdot (\kappa_i \nabla T_i) + \rho \kappa_{ei} \frac{(T_e - T_i)}{\tau_{ei}}$$

Radiation energy Density

$$\rho \frac{\partial u_R}{\partial t} = -\rho \vec{v} \cdot u_R + \frac{1}{3} u_R \nabla \cdot \vec{v} + \nabla \cdot (\rho \chi_{rad} \nabla u_R) + \Phi_{eR}$$

Magnetic Induction

$$\rho \frac{\partial \vec{B}}{\partial t} = \nabla \times (\vec{v} \times \vec{B}) - \nabla \times (\eta \vec{J}) - \nabla \times \left(\frac{\vec{J} \times \vec{B}}{e n_e}\right) + \nabla \times \left(\frac{\nabla P_e}{e n_e}\right)$$

Elastic Stress

$$\rho \frac{\partial \sigma^d_{ij}}{\partial t} = 2\mu d^d_{ij} - v^k \nabla_k \sigma^d_{ij}$$

The equations are closed with various equations of state and transport coefficient models. For the results presented here, a new tabular equation of state package, Aurora, was developed and implemented into Mach2. Aurora was designed to calculate the equilibrium thermodynamic quantities of dissociated and ionized polyatomic species, such as Teflon or polyethylene. The details of Aurora are to be discussed elsewhere.

Description of the Mk1 Gun Model

The physics include thermal diffusion, magnetic field diffusion, rlc circuit model with 5400 V, 660 μF capacitance, 180 nH external inductance, 1.0 mΩ external resistance, Teflon ablation along lower boundary of the trigger block, as indicated in Fig. 4 below. Initial global mass density of 1.5 E-4 kg/m3 with 7.54 E-6 in the trigger block. Initial global temperature of .025 eV (270 K) with 3.665 eV in trigger block. Figure 4 below shows the computational domain, along the right hand side of the axis of symmetry. The mirror of the domain is shown for visual reference. Eulerian grid.

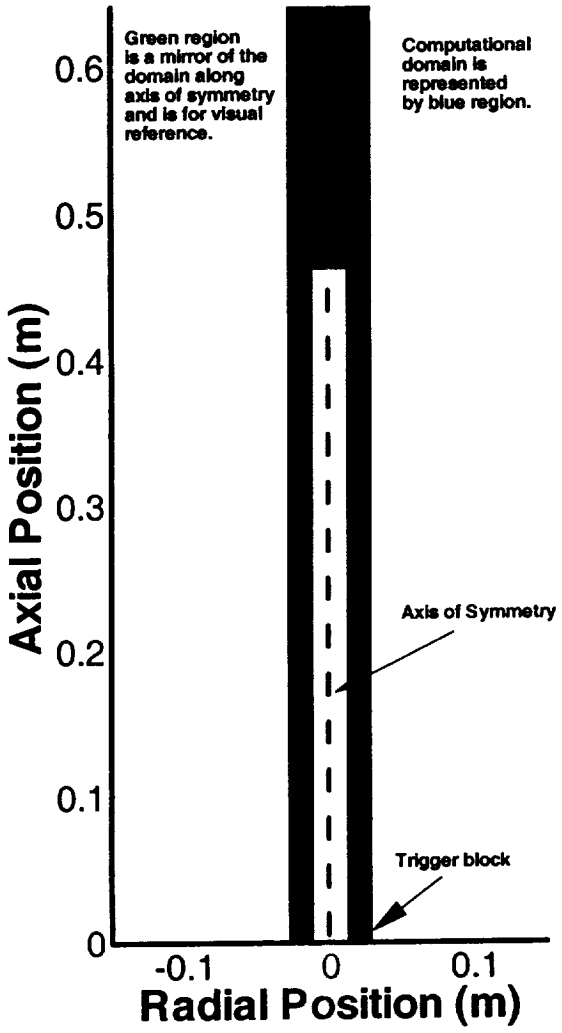

Figure 4. Computational Domain for MK1 Gun Runs.

Experimental Results

Bdot and light pipe probes were among the diagnostics used in the series of experiments with the Mark I coaxial plasma gun. The probe stations are as shown in Fig. 5.

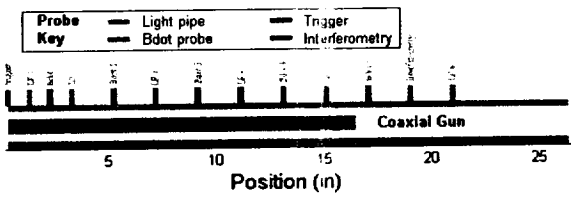

Figure 5. Probes as they were stationed along the Mark I gun.

The light pipes were positioned as shown in Fig. 5 and given in Table 1 below. A typical light pipe probe signal is shown in Fig. 6. A sharp rise in the signal indicates that a high temperature plasma is within the field of view of the probe. Because of some electrical problem with the photomultiplier tubes, the intensity of the signal does not necessarily correlate to the intensity of the signal. This problem is under investigation.

Probe Name	Position (in)
LP1	1.0
LP2	3.0
LP3	7.0
LP4	11.0
LP5	15.0
LP8	21.0
LP10	52.0

Table 1. Light pipe probe names and positions

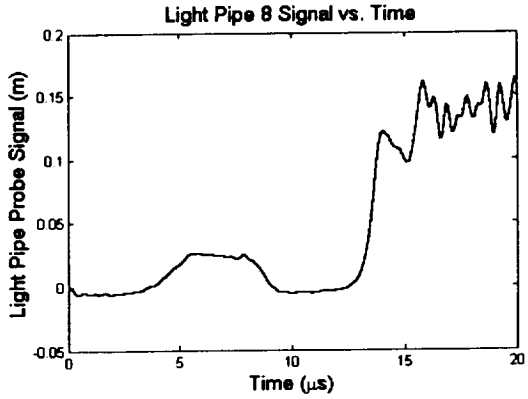

Figure 6. A typical light pipe probe signal.

A set of five Bdot probes were stationed along the length of the gun to measure the current as a function of position and time as shown in Fig 7. and Table 2. The probe names and positions

Bdot Probe	Position (in)
$B_{1\theta}$	2.0
$B_{2\theta}$	5.0
$B_{3\theta}$	9.0
$B_{5\theta}$	13.0
$B_{6\theta}$	17.0

Table 2. Bdot probe positions.

The Bdot probes were calibrated against a Rogowski belt with a known current to voltage output ratio. The uncertainty in the probes was less than 5%. The integrated signal for $B_{1\theta}$, the probe closest to the trigger, is given for a typical shot, Fig. 7.

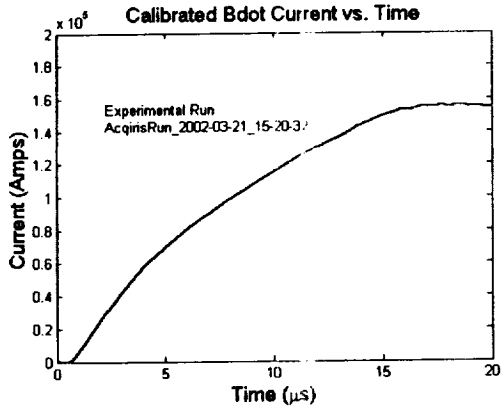

Figure 7. Current from the bdot probe $B_{1\theta}$, showing the current in the vicinity of the gun breech.

Figure 7 shows the current rises sharply from about 1 μs and peaks around 18 μs at about 155 kAmps. Figure 8 below shows scaled bdot probe currents as a function of position. This chart clearly indicates a current sheet propagating downstream. The run number is given for reference. From this figure one can estimate the velocity by dividing the distance between adjacent probes by time to a fraction of probe current peak.

Table 3 below is a calculation of velocity vs. bdot probe position for 10% of the peak current for each probe. The exit velocity of the gun is about 41 km/s. As a consistency check, one can repeat this calculation for the light pipe signals. Table 4 below is a summary of velocity vs. position for 10% of the peak light pipe signals. The exit velocity calculated from the light pipe probes is about 53 km/s, which is in fairly good agreement with the Bdot probe data.

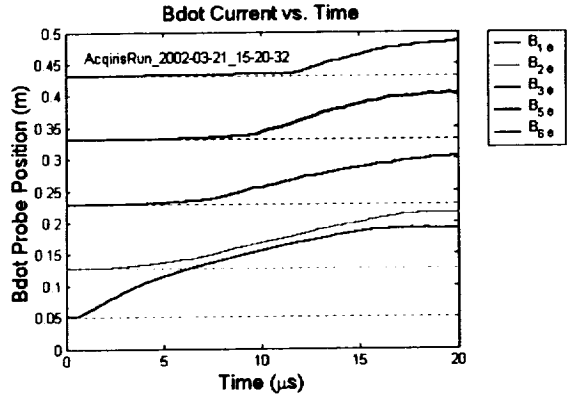

Figure 8. Bdot probe current as a function position along the coaxial gun.

Probe	Time (μs)	Velocity (m/s)
$B_{1\theta}$	1.55	32774.19
$B_{2\theta}$	5.05	52551.72
$B_{3\theta}$	7.38	29028.57
$B_{5\theta}$	9.81	43605.15
$B_{6\theta}$	12.07	41810.7

Table 3. Velocity calculated between adjacent bdot probes by dividing relative probe position by relative time to 10% of peak signal.

Probe	Time (μs)	Velocity (m/s)
LP1	1.39	18273.38
LP2	4.24	39379.84
LP3	6.36	35649.12
LP4	7.82	47924.53
LP5	10.68	69589.04
LP8	13.15	53286.71

Table 4. Velocity calculated between adjacent light pipe probes by dividing relative probe position by relative time to 10% of peak signal.

Comparisons of Mach2 with Experiment

Mach2 was run to simulate the Mark I coaxial gun experiments. Virtual bdot probes were set in the Mach2

run in the same positions as in the experiment. The current from $B_{1\theta}$ obtained with Mach2 is overlaid with the current $B_{1\theta}$ in the experiment, Fig. 9. Very good agreement is obtained between the two.

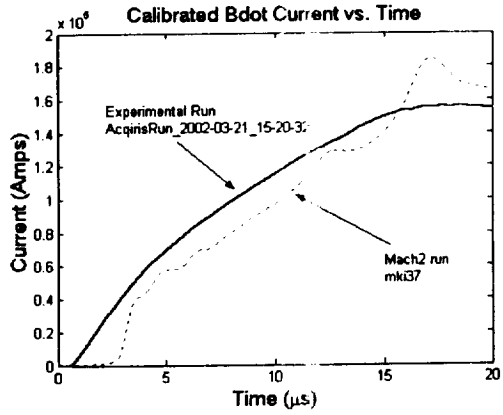

Figure 9. Comparison of Bdot probe data from experiment and Mach2 results.

Figure 10 is an overlay of all the probe currents as a function of position. Very good agreement is achieved between the experiment and theory, and is well within the uncertainty in the experimental measurements.

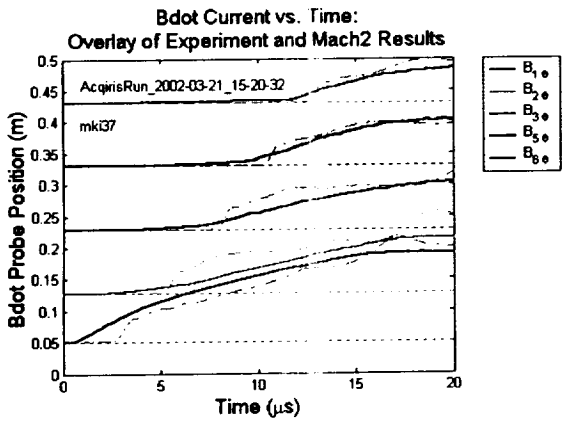

Figure 10. Bdot current as a function of probe position: comparison of experiment and Mach2 results.

Two Dimensional Mach2 results

With the accurate prediction of the current as function of position, one can examine the two dimensional plots of the plasmadynamic variables with confidence in the results. The results to follow in this section are vector and contour plots of current, velocity, density, temperature, and pressure, at 5 and 15 μs. Temperature is plotted in units of eV, and the rest of the variables are plotted in SI units.

As shown in Fig. 11, the current sheet forms in the trigger block, and diffuses downstream. After 5 μs, the current sheet has split into two distinct regions, one at the breech and one further downstream. By 15 μs, a major portion of the flux has reached the end of inner conductor, the probable location of the bulk, high velocity plasma flow.

The initial speed of the plasma is 118.6 m/s, as calculated from the analytical model. By 5 μs, a plasma jet has formed reaching speeds of about 50 km/s, which is consistent with the velocities calculated in the tables above for LP2 and $B_{1\theta}$, which are at about the same location as the jet in Figure. By 15 μs, portions of the jet have reached 80 km/s, although the leading edge is a more modest 30 km/s. The diffuse plasma exits at 50 km/s, which is also consistent with the velocity estimates in the tables above. The diffuse plasma is also in agreement with the LP8 signal, Fig. 6. Light pipe 8 is located downstream of the inner conductor, and remains illuminated for an extended length of time, suggesting a diffuse current sheet. Mach2 is consistent with that observation.

The density plots elucidate the bulk plasma motion over time. By 15 μs, the jet has reached the inner electrode, and by 20 μs, the jet begins to exit the gun.

The temperature contours tend to follow the current diffusion, since the main heating process is ohmic dissipation. Although some local hot spots can be as high as 15 eV, the plasma tends to hover around 4 eV. It should be mentioned that radiation is not turned on in the model, as the opacities have not been added to the Aurora equation of state package. It is expected that this temperature will be a bit lower once the radiation is accounted for.

The pressure plots do not add much more to the discussion of the results, but are included for completeness. The pressure contours follow the speed and current contours. The pressure at the breech is very high in comparison with the rest of the domain, due to high density material ablating off the wall. Otherwise, the plasma jet tends to be at about 0.01 to 0.1 atm.

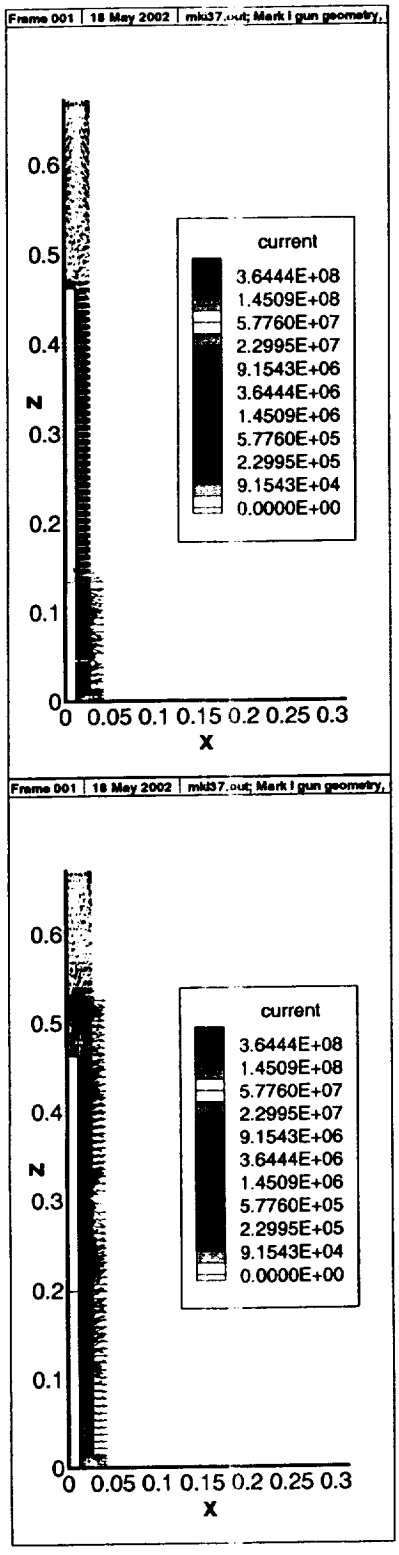

Figure 11. Current density vectors at 5 and 15 μs.

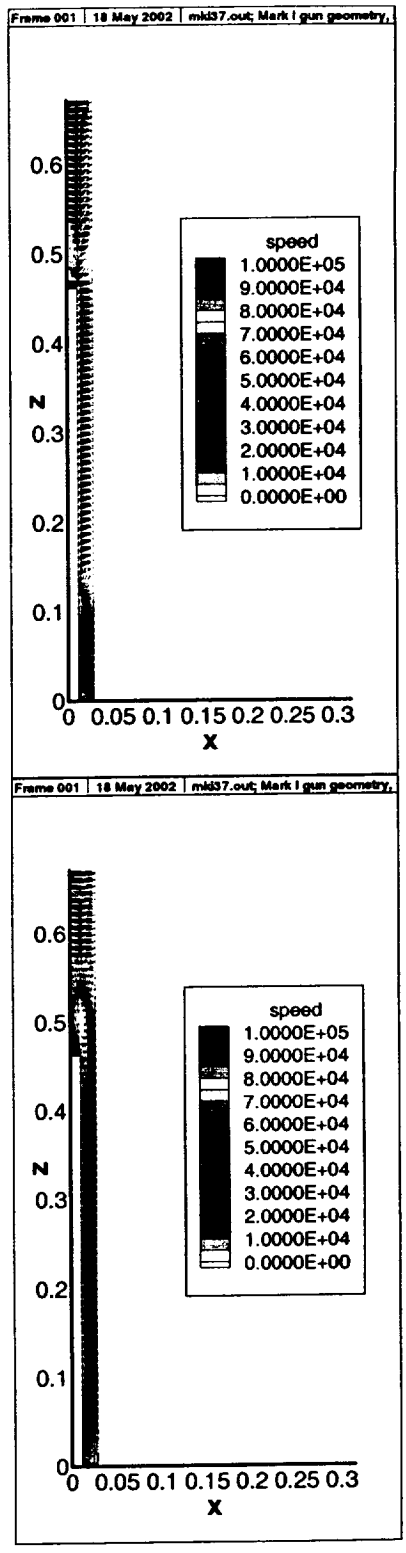

Figure 12. Velocity vectors from at 5 and 15 μs.

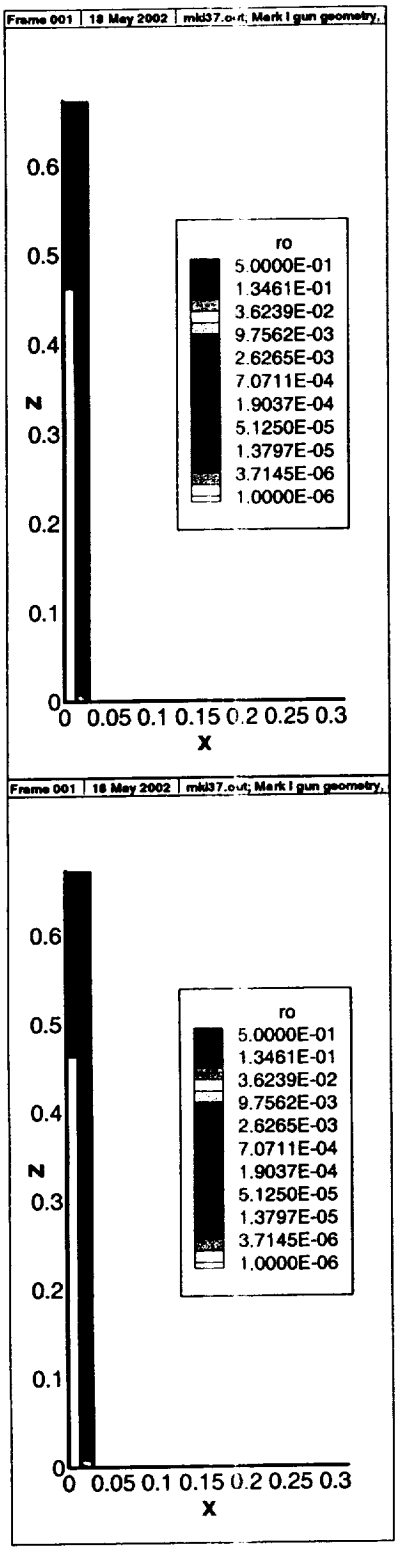

Figure 13. Mass density contours at 5 and 15 μs.

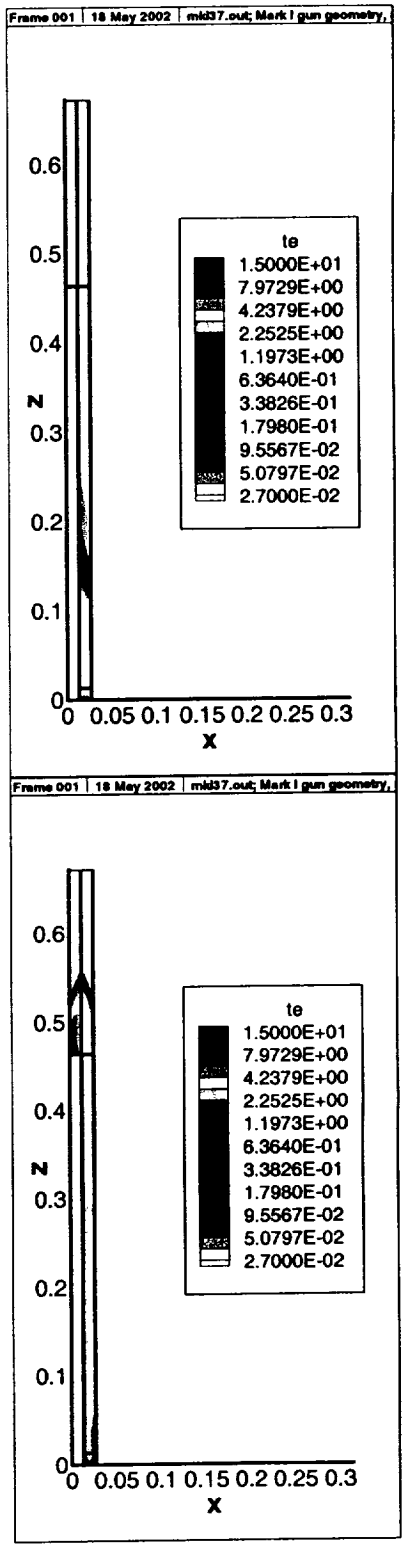

Figure 14. Temperature contours at 5 and 15 μs.

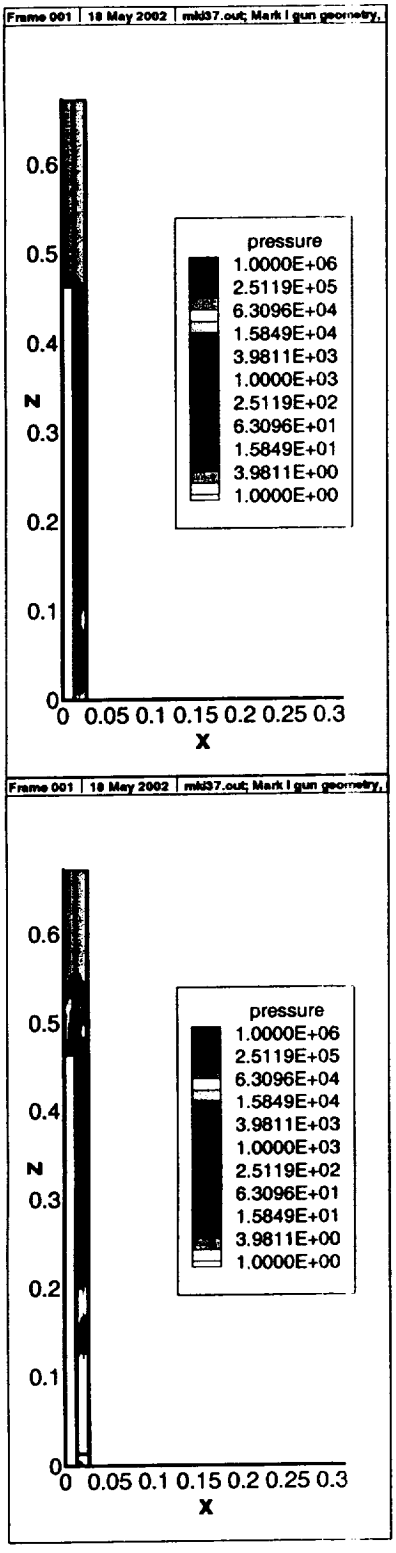

Figure 15. Pressure contours at 5 and 15 μs.

References

1. J.D. Filliben, *Electric Thruster Systems. Report CPTR-97-65.*, (Chemical Propulsion Information Agency, John Hopkins University, Columbia, MD, USA, 1997), p. 168.
2. R.L. Burton and P.J. Turchi, "Pulsed Plasma Thruster," *Journal of Propulsion and Power* **14,** 716 (1998).
3. P.J. Turchi, "Directions for Improving PPT Performance," *International Electric Propulsion Conference* (1997, 1997).
4. D. Keefer and R. Rhodes, "Electromagnetic Acceleration in Pulsed Plasma Thrusters," *International Electric Propulsion Conference* (1997, 1997).
5. R.E.J. Peterkin, J.H. Degnan, T.W. Hussey, N.F. Roderick, and P.J. Turchi, "A Long Conduction Time Compact Torus Plasma Opening Switch," *IEEE Transactions on Plasma Science* **21,** 522 (1993).
6. P.G. Mikellides, *A Theoretical Investigation of Magnetoplasmadynamic Thrusters*, Ph. D. Dissertation Thesis, Ohio State University, 128 pages (1994).
7. P.G. Mikellides, P.J. Turchi, and N.F. Roderick, "Applied-Field Magnetoplasmadynamic Thrusters, Part 1: Numerical Simulations Using the MACH2 Code," *Journal of Propulsion and Power* **16,** 887 (2000).
8. P.G. Mikellides and P.J. Turchi, "Applied-Field Magnetoplasmadynamic Thrusters, Part 2: Analytic Expressions for Thrust and Voltage," *Journal of Propulsion and Power* **16,** 894 (2000).
9. P.G. Mikellides, P.J. Turchi, and N.F. Roderick, "Analysis of Applied-Field Plasma Thrusters Using the Mach2 Code," 1994, 1994).
10. P.G. Mikellides, P.J. Turchi, and N.F. Roderick, "Theoretical Model for Applied-Field MPD Thrusters," *31st AIAA/ASME/SAE/ASEE Joint Propulsion Conference and Exhibit* (San Diego, CA, July 10-12, 1995, 1995).
11. Z.-G. Shen, C.-H. Liu, C.-H. Lee, C. Wu, and S. Yang, "A Study of a Coaxial Plasma Gun," *Journal of Physics D: Applied Physics* **28,** 314 (1995).
12. K. Sankaran, E.Y. Choueiri, and S.C. Jardin, "Application of a new Numerical Solver to the Simulation of MPD Flows," *36th AIAA/ASME/SAE/ASEE Joint Propulsion Conference and Exhibit* (Huntsville, AL, July 16-19, 2000, 2000).

13. M. Andrenucci, M. Caprili, and R. Lazzeretti, "Theoretical Models for Plasma Motion in Pulsed Coaxial Hydromagnetic Guns," *39th Meeting of the Advisory Group for Aerospace Research and Development Propulsion and Energetics Panel* (USAF Academy, Colorado Springs, CO, June 12-15, 1972, 1972).
14. T. Ao and T. Fujiwara, "Numerical and Experimental Study of an MPD Thruster," *17th International Electric Propulsion Conference* (Tokyo, Japan, 1984).
15. Y.C.F. Thio, C.E. Knapp, R.C. Kirkpatrick, R.E. Siemon, and P.J. Turchi, "A Physics Exploratory Experiment on Plasma Liner Formation," *J. Fusion Energy* (2002, to appear).
16. G.W.C. Kaye and T.H. Laby, *Tables of Physical and Chemical Constants, 10th edition* (Longmans, Green & Co., London, 1948).